POROSITY AND PERMEABILITY ANALYSIS ON NANOSCALE FIB-SEM 3D IMAGING OF SHALE ROCK

Shawn Zhang, Visualization Sciences Group - VSG
Robert E. Klimentidis, ExxonMobil Upstream Research Co.
Patrick Barthelemy, VSG

This paper was prepared for presentation at the International Symposium of the Society of Core Analysts held in Austin, Texas, USA 18-21 September, 2011

ABSTRACT

As oil and gas production from conventional reservoirs is declining and oil price is going up, unconventional mudstone reservoirs ("shale-gas") are becoming more important. However, while their characterization is of utmost importance for production planning, these low permeability rocks are very challenging to characterize due to their complex nano-scale pores and mineral structure. 3D imaging is a critical tool in the visualization, analysis and modeling of these type of reservoirs.

In this study, FIB-SEM (Focused Ion Beam - Scanning Electron Microscopy) 3D imaging at 5nm pixel resolution was used to study porosity, connectivity, and to model permeability of a mudstone core sample extracted from a production well in North America. With 3D reconstruction, extraordinary detail of the pore space in both the mineral and organic matter phases can be visualized and analyzed. Advanced image analysis algorithms were used to extract volumes of the different phases and to compare these with the physical laboratory experiments of porosity and permeability. Special focus was placed on the impact of pore space in the organic matter. These pores tend to be larger than the other pore types. The impact of segmentation procedure on porosity calculation was systematically studied.

Segmented FIB-SEM images are used as the input to the Stokes flow solver to simulate viscous fluid flow through the rock. The simulation results can be compared with physical laboratory experiments.

In addition to analysis of mudstone samples, the workflow proposed by this study is potentially applicable to a wide range of core sample and more general porous material analysis.

1. Introduction

Oil and gas production from conventional reservoirs is declining and oil price is rising. Unconventional mudstone reservoirs, sometimes called “shale-gas” reservoirs are becoming more important. In addition, the nuclear power plant failure in Japan caused by the earthquake and subsequent tsunami is making nuclear power related decisions more difficult and other energy sources, including natural gas confined in shale rock, even more attractive.

Mudstone reservoir rocks are very challenging to characterize due to their complex nano-scale porosity and mineral structure. 3D imaging from X-ray and SEM at very high resolution is becoming more important in the visualization and characterization of these reservoirs.

Typical analysis techniques for shale-gas reservoir rocks include: total organic carbon (TOC), X-ray diffraction, absorbed/canister gas, vitrinite reflectance, detailed core and thin section descriptions, porosity, permeability measurements, fluid saturation, and optical and electron microscopy [8] . These sample-based results are combined with full well-log suites, including high resolution density and resistivity logs and borehole images, to fully characterize these formations. Porosity, fluid saturation, and permeability derived from core can be tied to log response; however, several studies have shown that the results obtained from different core analysis laboratories can vary significantly, reflecting differences in proprietary analytical protocols, differences in definitions of fundamental rock and fluid properties, or the millimeter-scale variability common in mudstones that makes it problematic to select multiple samples with identical attributes.

Extensive observations on 2D SEM images have been performed [5] on broad ion milled samples. These studies reveal the presence of porosity in mineral matrix, and in organic matter. The development of porosity in organic matter is not yet well understood but is most likely related in part to organic matter maturity and types.

In this study, three dimensional focused ion beam - scanning electron microscopy (FIB-SEM) [4] imaging was used to study porosity, connectivity, and permeability of a mudstone core sample extracted from a production well in North America at 5nm resolution. The third dimension revealed large amount of new information [10]

With 3D reconstruction, extraordinary detail of the pore space in both the mineral and organic matter phases can be visualized [14] . Advanced image analysis algorithms are used to extract volumes of the different phases and to compare these with the physical laboratory experiment results of porosity and permeability. Special emphasis was placed

on the impact of pore space in the organic matter. These pores tend to be larger and better connected than the other pore types. The impact of segmentation procedure on calculation of porosity was systematically studied.

Geometry or image based simulation approaches can be used to model the permeability of the sample. In the geometry based approach, surface geometries corresponding to pore space are explicitly reconstructed. A volumetric mesh representing the pore space is built for a computational fluid dynamics simulation based on Navier-Stokes equations. While this approach is conceptually feasible [14] , it is computationally prohibitive to solve flow through millions of pores at micro or nano scale. In this paper, a nova image based simulation approach is presented. Binarized FIB-SEM images masking the pore space are the input to a Stokes flow solver. The simulation results can be compared with each other as well as physical laboratory experiments. The impact of connectivity on petrophysical properties will be investigated.

In addition to analysis of mudstone samples, the workflow proposed by this study is potentially applicable to a wide range of core sample and more general porous material analysis [11] [13] .

2. Image acquisition & processing

Figure 1 shows one of the rock samples under study. Thin sections (Figure 1a) are extracted from the core sample of a North American mudstone reservoir. A close up on the yellow box area is shown in Figure 2b using light microscope. It is clear that porosity cannot be detected. A further close up on the yellow box is shown in Figure 2c using SEM, which reveals the pores, organic matter and mineral matrix at nano scale.

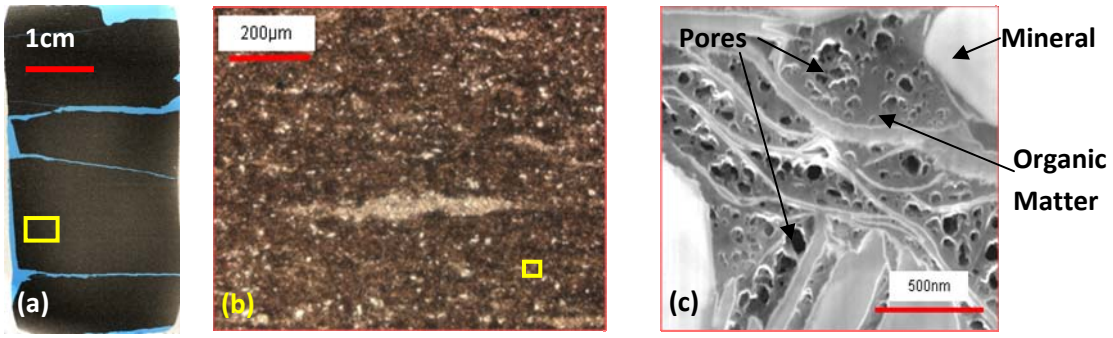

Figure 1. A sample shale gas rock. (a). Optical photograph of the whole thin section. (b). Close up of yellow box in (a) with light microscope under plain light. (c). Close up of the yellow box in (b) with SEM.

If we combine the SEM scanning column with a Ga-Focused Ion-Beam column, we are able to iteratively mill away thin serial slices and take SEM pictures of each slice. This

results in a stack of 2D SEM images. These images can be used to reconstruct a digital 3D volume which contains mineral matrix, organic matter, and pores information as different intensity ranges. In our case, a sample 9.895 micron by 8.645 micron by 5.42 micron in size is studied. This sample is represented digitally with 4 billion voxels, which is a significant amount of data. To correct the noise and stage drifting, a median noise reduction filter and a least square based automatic alignment procedure are employed [14]

Figure 2 shows the reconstructed 3D volume. Image is enhanced with noise reduction and drift correction, and rendered using interactive volume rendering technology accelerated by a graphics processing unit [6] .

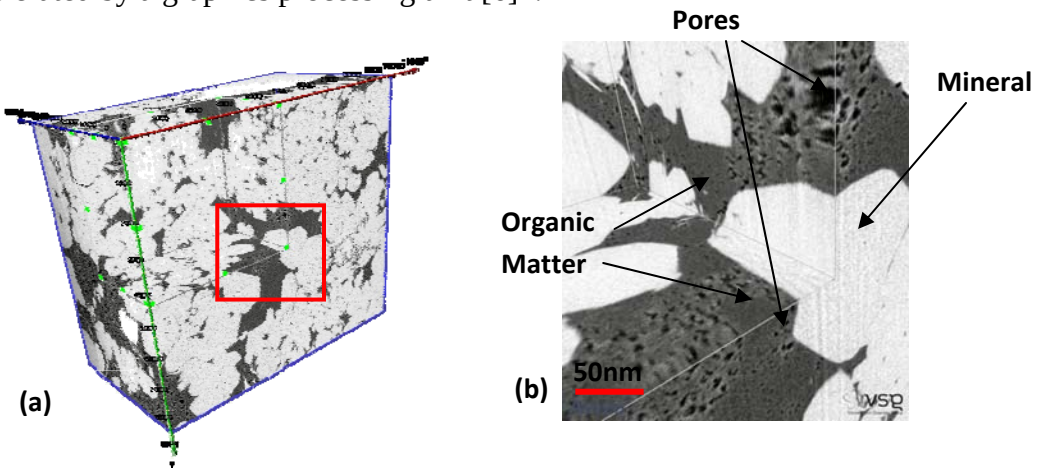

Figure 2. (a). 3D rendering of reconstructed shale rock volume. Scale is in nanometers. (b). A close-up view of the area highlighted by the red box in Figure 2a.

3. Image segmentation: mineral, organic matter and porosity volumes definition

3.1. Total organic matter network

The first step in the image segmentation process is separating the organic matter network from the mineral matrix. Then the non-percolating portion is removed. This porous network, within organic matter, dictates the main oil and gas flow orientation around the mineral matrix.

Figure 3 illustrates the procedure that we used to segment the organic matter network. Starting from a median filtered 3D image data (Figure 3a), a simple threshold is first performed to mask out voxels belonging to the higher intensity mineral matrix (Figure 3b). Then an algorithm examines all voxels that do not belong to the mineral matrix, to remove those that are not in continuity. Small clusters of organic matter fully enclosed within the mineral matrix, as well as small isolated pores in the mineral matrix, are

removed because they are not contributing to the permeability (Figure 3c). At this stage we have a blue mask of mineral matrix and everything non-percolating. If we invert the mask (changing everything black to blue), we obtain a mask of percolating organic matter, which we can logically multiply with the original data to get an image with only percolating organic matter.

Table 1 summarized the measured volume percentages. Total non-mineral material volume percentages, based on Figure 3b, is 24.2%. This includes total pore volume (mineral pore and organic matter pore) and organic matter volume.

The percolating organic matter volume percentage is 24.1%. Non percolating organic matter only accounts for 0.1% of the total volume, which leads to the conclusion that the organic matter network is well connected.

An important assumption introduced in this procedure is that there are no nanoscale pore throats with size smaller than 5nm. This assumption is imposed by the FIB-SEM image acquisition resolution limit.

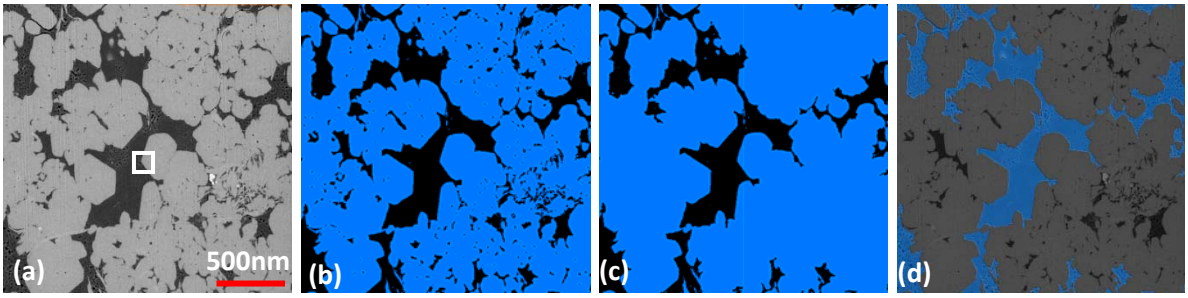

Figure 3. Segmentation of organic matter network. (a) Median filtered data; (b) Simple intensity threshold between 120-255 to mask out mineral matrix; (c). Remove organic matter that is not part of a percolating network (Note this step is made more dramatic to show the difference); (d). Invert the mask to identify the percolating organic matter.

3.2. Pore volume percentage

Segmentation of the pore network is probably one of the most important yet the most challenging step in a 3D imaging study. In Figure 4a, a close-up of one slice of the original data corresponding to Figure 3a is shown. We can see the dark areas representing pore space. There are also a large number of isolated, small, dark pixels (yellow arrows in Figure 4a). We are not sure whether these are imaging artifacts or they are actual pores. In this study, we assume the pores are at least 2-3 voxels (10-15 nm) in size.

Even for bigger pores, ambiguities exist. We create a line probe crossing two obvious pores, and plotted intensity value in Figure 4b labeled as curve 1. Four valleys,

corresponding to the four pores with different darkness and different size, are identified and labeled with blue arrows. Three different segmentation strategies, top hat [12] (Figure 4c), threshold between 0-50 (Figure 4d) and threshold between 0-53 (Figure 4c) all reveal some correct pore space. While Figure 4e identified all four valleys, as labeled by blue arrows, it over estimates significantly the top valley (marked A), while picking up a lot of background noise (marked B).

Table 1. Petrophysical parameters calculated in this project.

Volume percentage	Values
1.Total non-mineral	24.2
2.Percolating organic matter and porosity	24.1
3.Total porosity	6.25
4.Percolating porosity	5.3

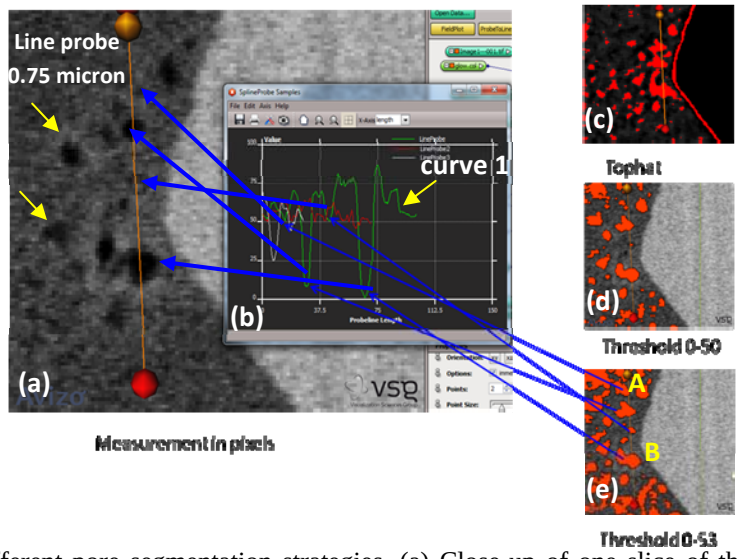

Figure 4 (Above right). Different pore segmentation strategies. (a) Close-up of one slice of the original data (white box in Figure 3a). (b) A profile of intensity values along the line probe defined in Figure 4a. (c) Top hat segmentation, overlain on Figure 4a. (d) Threshold segmentation using intensity range between 0 and 50. (e) Threshold segmentation using intensity range between 0 and 53.

We systematically studied the effect of different thresholds on the pore space, using the whole dataset, as well as each octant of the original data after it is divided into 8 equal sub-volumes. All results are plotted in Figure 5. The range of the threshold being studied is from 10 to 100, though we know only range 45-65 gives reasonable results.

For the whole data set (black curve with square symbols), we see porosity changed from about 4% to about 13% when threshold increases from 45 to 65. Similar dramatic jumps are observed on the octants. Not surprisingly, porosity measurement is very sensitive to the threshold value.

Given the same threshold, for example, 65, we can see different octants showing very different porosity, from 7% (Octa4) to 19% (Octa2). This shows significant anisotropy within the sample.
Due to the lack of consistency with threshold approach, we introduced top hat segmentation [12] , and performed a similar study.

Top hat filter has several steps, as shown in Figure 6.

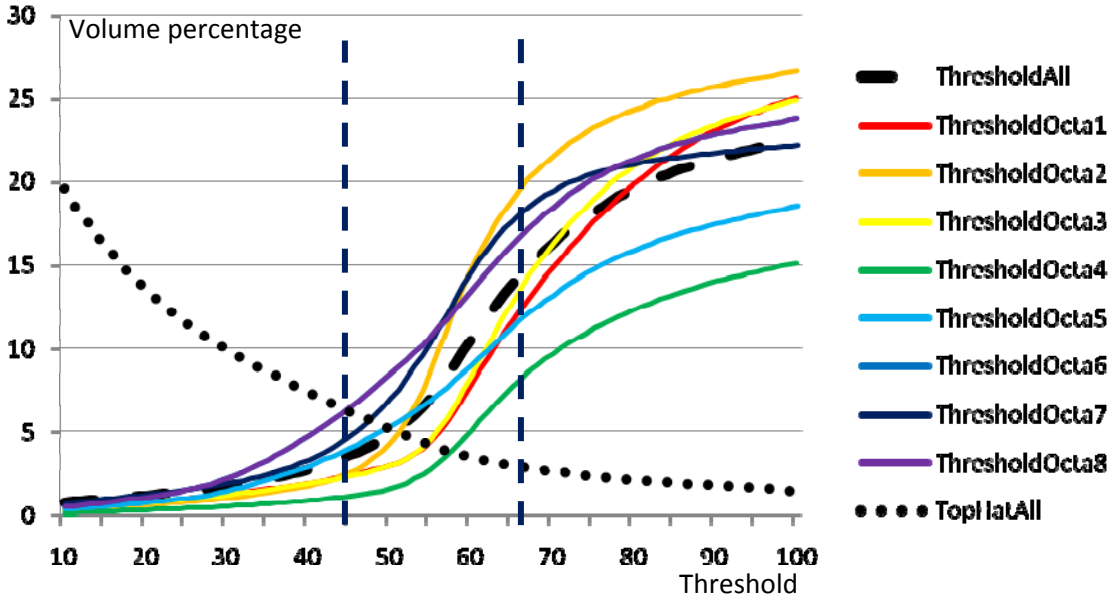

Figure 5. Thresholding and pore space volume percentage. Top hat results (thick black curve with circle symbol) is plotted as a reference. (For best clarity, please refer the color pictures in conference proceeding CD).

A threshold is still necessary at the last step, however, it will be able to pick up peak (or valley) based on a local criteria.

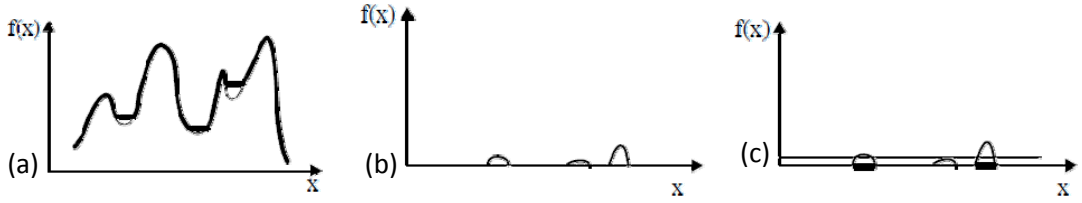

Figure 6. 1D illustration of top hat procedure. (a) Closing. (b). Original result minus Figure 6a. (c). Threshold on Figure 6b.

Figure 7 shows sensitivity of porosity measurement based on top hat threshold. Top hat threshold variation from 45-65 causes porosity variation from 7% to 3.5%, which is smaller than the porosity variation corresponding to simple threshold. Similarly, for different octants, porosity varies from 3.5% to 6.5% at top hat threshold value 45.

While Top hat is established as a more reliable approach, we took advantage of both approaches by combining the results of a low simple threshold (0-50) and top hat. This gives the most accurate segmentation results, with porosity calculated at 6.25% (Table 1).

Within the porosity in organic matter, most of it (5.3% of total volume) is percolating. Figure 8 shows a snapshot of one slice of the segmentation results.

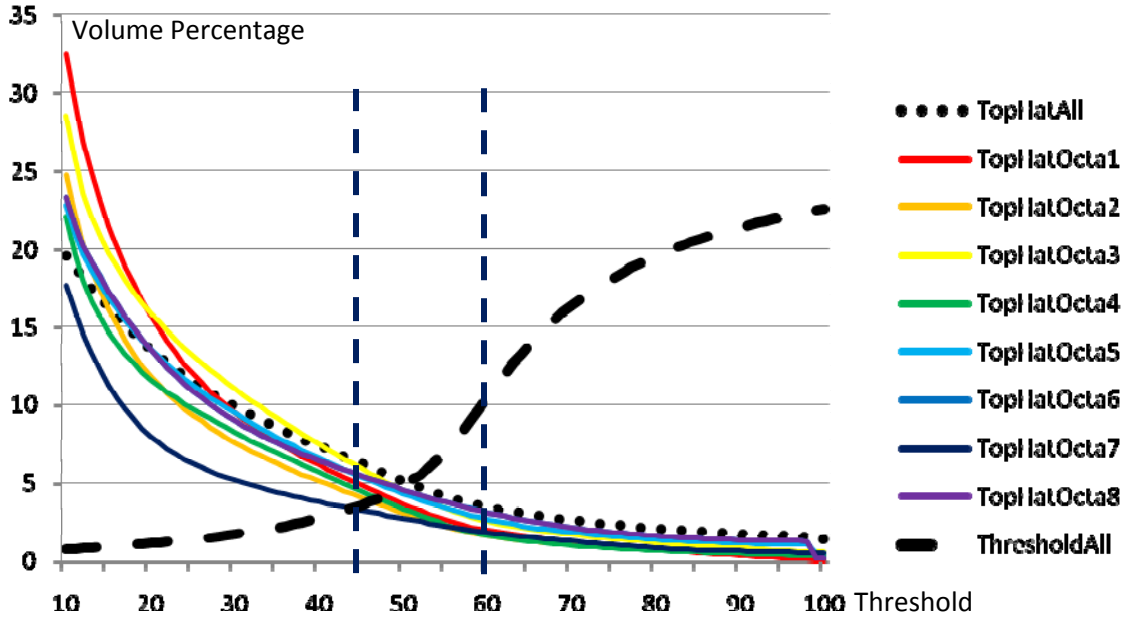

Figure 7. Top hat thresholding (X-axis) and pore space volume percentage (Y-axis). Simple threshold results (thick black curve with square symbol) is plotted as a reference. (For best clarity, please refer the color pictures in conference proceeding CD).

4. Permeability

4.1 New Stokes permeability solver and its validation

A new flow solver, Avizo XLab, was developed based on Avizo [1] visualization and data analysis framework. This flow solver solves 3D Stokes equation using the image segmentation results, as shown in Figure 9a. Fluid flow first enters a divergence channel (marked "inflow" in figure 9a), before it hits the porous material. Likely, the flow exiting the material first enters a convergence channel (marked "outflow" in figure 9a) before it is released. The inflow and outflow zone are added to accommodate the complex porous shape of the sample faces where the fluid goes in and out, to increase numerical stability.

The segmented image (often referred to as labels) gives a staggered grid. An artificial compressibility scheme [2] is employed to solve pressure (at the center of the grid) and velocity (at the boundary of the grid), as shown in Figure 8b. After the flow field is resolved, Darcy's law is used to derive permeability [9] . This new flow solver is validated against a few basic geometries, with reasonably accurate results summarized in Table 2. Note the first two experiments are measured on pixels.

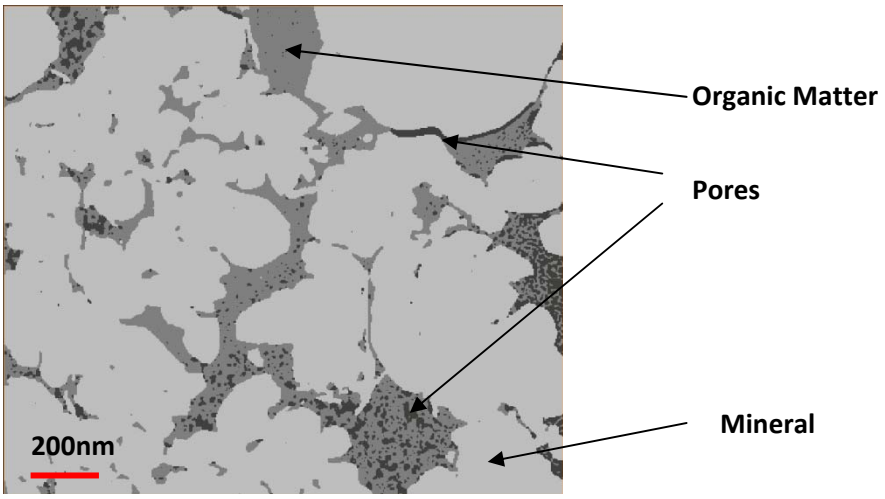

Figure 8. 2D slice of the final segmentation results.

4.2. Pore space characterization

The permeability simulation is performed along three axes. Figure 10 shows the simulation setup, pressure solution and velocity solution in the X direction.

The permeability simulation results are summarized in Table 3. The sample is permeable in all three directions.

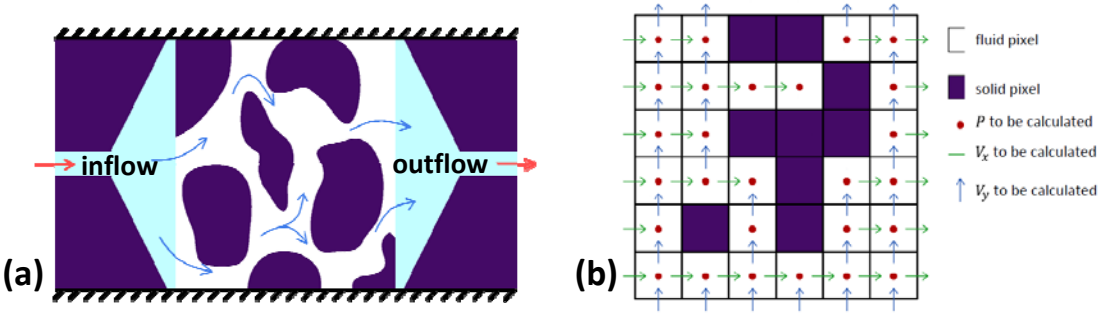

Figure 9: (a). 2D illustrations of the simulation setup. (b). 2D illustration of physical properties solved and their locations in the staggered grid.

Two permeabilities are calculated for each direction, one for the network of percolating organic matter (labeled as total pore perm in Table 3), and one for all percolating pores (labeled organic matter perm in Table 3). Total pore perm is defined as the permeability measured on all percolating pores, with corresponding porosity measured in Table 1.4. Organic matter perm is the permeability measured by assuming all organic matter is void, with corresponding volume percentage measured in Table 1.2. Organic matter perm may be important when all organic matter is dissolved. The organic matter perm ranges between 100-200 microdarcies, while the total pore perm ranges from 200 to 900 nanodarcies. This is in the range of some analysis laboratory measurements of these

rocks. Note all permeability simulations are done under unit pressure drop and unit viscosity.

Table 2. Permeability validation on the new Avizo Xlab Stokes flow solver (D stands for darcy, which is approximately 10^{-12} m^2 [9])

Case	Theory	Theory value	Xlab value
Square Cylinder, Side length **b**=25 pixel	**$K=0.422b^2/12$ [7]**	21.979 $pixel^2$	21.91 $pixel^2$
Round cylinder Radius **r**=25 pixel	**$K=r^2/8$ [7]**	78.125 $pixel^2$	78.439 $pixel^2$
MicroCT scan of glass packaging with spherical particles diameter **d**= 100-120um, material porosity **ε**=36.5, 400x400x400	Kozeny-Carman equation[3] : $K=\frac{1}{180}\frac{\varepsilon^3}{(1-\varepsilon)^2}d^2$	6.7-9.7 um^2 (6.6-9.6 D)	7.8um^2 (7.7 D)

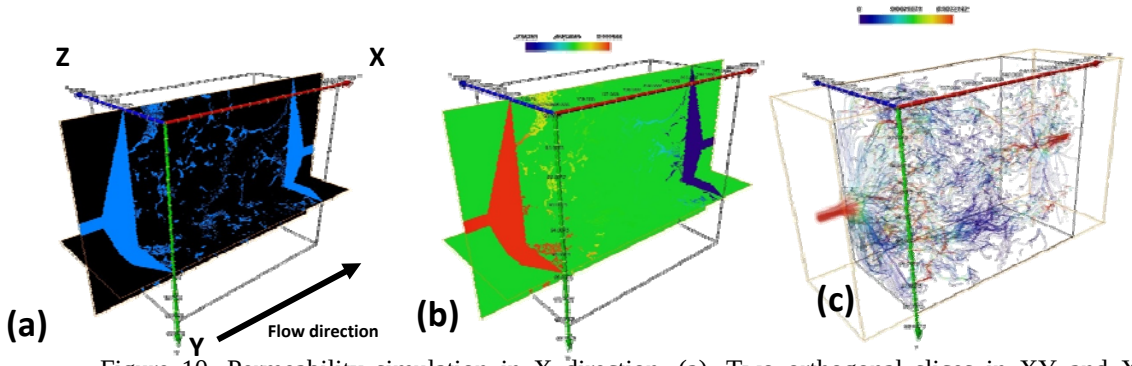

Figure 10. Permeability simulation in X direction. (a). Two orthogonal slices in XY and XZ direction showing simulation setup for the pore network. (b). Two orthogonal slices in XY and XZ directions showing pressure distribution. (c). Illuminated streamlines, colored by velocity magnitude, showing the velocity solution.

We believe the permeability simulation results are underestimates of reality, due to at least two reasons. First of all, the imaging resolution (5nm), though accurately capturing all of the pores, might not be enough to capture capillary pore throats below 10-15nm. The insufficient resolution is not significant for porosity estimation as nano-scale throats are only a tiny fraction of total porosity. However, for permeability estimates, insufficient resolution becomes an issue as these nano-scale pore-throats may actually be the major percolating pathways. The impact is greater for the permeability model based on the porosity as compared to the permeability model based on the network represented by the organic matter volume where the flow channels are much bigger (as we assumed all organic matter occupied space are voids).

Table 3. Permeability results

	Percolat-ing	Total pore perm (nD)	Organic matter network perm (nD)	Shortest path (μm)	Shortest path/thickness	Longest path (μm)
X	Yes	828	156,000	11.29	1.141	14.18
Y	Yes	936	106,400	9.77	1.13	12.48
Z	Yes	280	224,400	5.84	1.08	9.49

Better resolution scans to understand the pore throat size, as well as the effort to model these throats, are underway.

The second factor is molecular diffusion, which can happen in pore space, organic matter, and mineral matrix. This is currently being developed, hence is not part of the simulation model used in this paper.

Along with permeability measures, a number of important porosity connectivity characteristics are calculated and shown in Table 3, including the shortest and longest permeable paths along each dimension. The ratio of shortest path to the length of the sample is an indicator of tortuosity.

Figure 11 shows the length of permeable path distribution in the whole sample along the three different directions. The length is shorter (blue) close to the entry where the calculation begins. As the algorithm traverses through the porous network, the path becomes longer. Some paths branch, while others hit dead-ends. However, in all three directions, many paths are identified that traverse through the rock, as indicated by the reddish color.

5. Conclusions and future work

FIB-SEM imaging was used to capture rock structure at the nano-scale. A toolbox of image processing, visualization, modeling and analysis software [1] was able to extract large amount of qualitative and quantitative information, based on which petrophysical parameters such as porosity, connectivity, and permeability can be calculated.

Special attention was paid to the image segmentation process. Image segmentation parameters can have a significant impact on the porosity calculation and permeability simulation results. Top hat segmentation along with threshold segmentation was shown to be more reliable.

Validation of these results with physical core laboratory experiments is underway, along with efforts of applying these results to shale reservoir modeling.

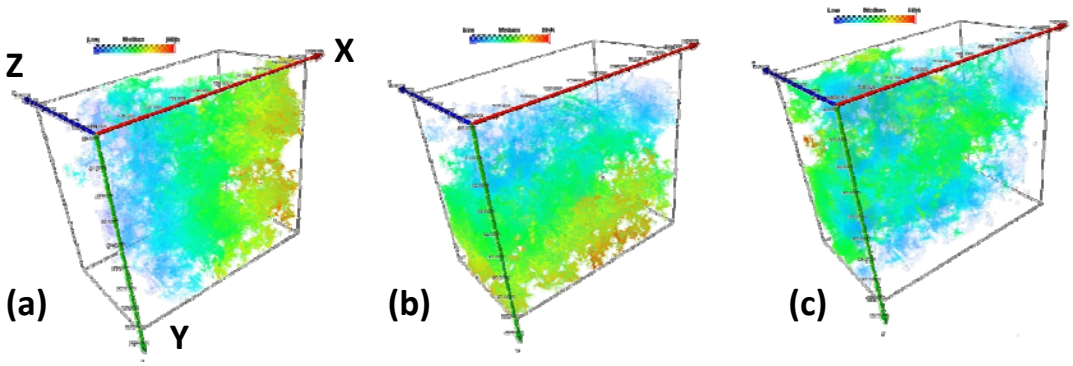

Figure 11. Permeable path distribution. (a). Along X direction; (b). Along Y direction; (c). Along Z direction. Redish color represents longer path.

References

[1] Avizo Software, 2011. VSG Website [Online] (Updated May 2011) Available at: http://www.vsg3d.com/avizo/overview [Accessed 13 May 2011].

[2] Chorin, A. J. "A Numerical Method for Solving Incompressible Viscous Flow Problems". *Journal of Computational Physics* , (1967)**2**, 12-26.

[3] Combaret, N., Albou, R., Lichau, D., Doux, P. & Bernard D. "Virtual Studio for Material Characterization". Poster at *3D Imaging of Materials Systems Workshop* (2010), Bordeaux, France.

[4] Giannuzzi, L.A. & Stevie F.A. *Introduction to Focused Ion Beams* (2005), Springer, NY.

[5] Klimentidis, R., Lazar, R., Bohacs, K.M., et al. "Integrated Petrographic Characterization of Mudstones". In *Proceedings of Annual American Association of Petroleum geologist Conference* (2010), New Orleans (Abstract).

[6] LaMar, E., Hamann, B., & Joy K. Multiresolution Techniques for Interactive Texture-Based Volume Visualization. In *Proceedings of IEEE Visualization* (1999), pp 355-361.

[7] Llewellin, E. W. "LBflow: An extensible lattice Boltzmann framework for the simulation of geophysical flows. Part II: usage and validation". *Computers & Geosciences*, **(**2010)36:123-132.

[8] Passey, Q.R., Bohacs, K.M., Esch, W.L., Klimentidis, R. et al. "From Oil Prone Source Rock to Gas-Producing Shale Reservoir - Geologic and petrophysical characterization of unconventional shale-gas reservoirs". *Society of Petroleum Engineers International conference* (2010), Beijing, China 8-10 June 2010.

[9] Permeability Wikipedia page. Wikipedia Website [Online] (Updated September 2010) Available at: http://en.wikipedia.org/wiki/Permeability_(earth_sciences) [Accessed 15 December 2010].

[10] Sondergeld, C.H., R.J. Ambrose, C.S. Rai, J. Moncrieff. "Micro-structural Studies of Gas Shales", SPE 131771, In Proceedings of SPE Unconventional Gas Conference, Pittsburgh, PA, USA, 2010.

[11] Takhar, P.S. & Zhang, S. 2009. Drying of Corn Kernels: From Experimental Images to Multi-scale Multi-physics Modeling. In *Comsol Conference Proceeding 2009*, Boston, MA, USA.

[12] Visilog reference guide. 2011.

[13] Zhang, S., Barthelemy P & Noel, J. "Advanced 3D Data Analysis and Visualization in Aluminum Die Casting using Computed Tomography". In *Proceeding of Materials Science & Technology Conference* (2009), Pittsburgh, PA, USA.

[14] Zhang, S., Maestra, F.D., Combaret, N., Klimentidis, R., Barthelemy, P., Albou, R., Lichau, D. & Bernard, D. "The Analysis and Simulation of Rock Properties Using FIB-SEM and Virtual Material Studio". *Proceedings of NAFEMS World Congress* (2011), Boston, USA, May 22-26, 2011.